Characterization of nanoporous Al 2 O 3 films at terahertz frequencies

Min Zhai, A. Locquet, Mi I Jung, Deokha Woo, D. S Citrin

▶ To cite this version:

Min Zhai, A. Locquet, Mi I Jung, Deokha Woo, D. S Citrin. Characterization of nanoporous Al 2 O 3 films at terahertz frequencies. Optics Letters, 2020, 45 (14), pp.4092. 10.1364/OL.390129 . hal-02993290

HAL Id: hal-02993290

https://hal.science/hal-02993290

Submitted on 6 Nov 2020

HAL is a multi-disciplinary open access archive for the deposit and dissemination of scientific research documents, whether they are published or not. The documents may come from teaching and research institutions in France or abroad, or from public or private research centers.

L'archive ouverte pluridisciplinaire **HAL**, est destinée au dépôt et à la diffusion de documents scientifiques de niveau recherche, publiés ou non, émanant des établissements d'enseignement et de recherche français ou étrangers, des laboratoires publics ou privés.

Characterization of nanoporous Al_2O_3 films at terahertz frequencies

MIN ZHAI,[1] A. LOCQUET,[1] MI JUNG,[2] DEOKHA WOO,[3] AND D. S. CITRIN[1,*]

[1]*Georgia Tech-CNRS UMI 2958, Georgia Tech Lorraine, 2 Rue Marconi, 57070 Metz, France and School of Electrical and Computer Engineering, Georgia Institute of Technology, Atlanta, Georgia 30332-0250 USA*
[2]*Konkuk University Glocal Campus, 268 Chungcheonbuk-do, 27478 Republic of Korea*
[3]*Sensor System Research Center, Korea Institute of Science and Technology, Seoul, Republic of Korea*
**david.citrin@ece.gatech.edu*

Received XX Month XXXX; revised XX Month, XXXX; accepted XX Month XXXX; posted XX Month XXXX (Doc. ID XXXXX); published XX Month XXXX

THz birefringence in nanoporous Al_2O_3 films grown on Al substrates characterized nondestructively by polarization-resolved THz spectroscopy. Sparse deconvolution is used to find the film thicknesses from the data, showing good agreement with the values measured directly by destructive cross-sectional field-emission scanning electron microscopy.

OCIS codes: Terahertz imaging; Nondestructive evaluation; Nanoporous Alumina; Time domain reflectometry; Birefringence.

http://dx.doi.org/10.1364/OL.99.099999

Nanoporous (NP) materials, with high surface-to-volume ratios, pore-size tunability, the possibility of periodic pore structures, and ease of functionalization, are emerging as promising structures for templates for subsequent fabrication, as matrices for biological growth, and as substrates for catalysis [1],[2]. While characterization at the nanoscale is clearly of great importance, these materials also exhibit important macroscopic properties that must be characterized. NP alumina (Al_2O_3), due to its large band gap (6.8 eV), dielectric constant, and mechanical strength, is of interest for thermoelectric devices and energy harvesting [3]. NP Al_2O_3 consists of a hexagonal array of air holes in Al_2O_3 film grown on Al substrate. Pore diameter, lattice constant, and depth are controlled by fabrication conditions [4][5]. Due to crystal and NP lattice anisotropy, such materials exhibit birefringence Δn. THz Δn has been observed in various systems [3],[6], [7],[8],[9],[6],[10],[11],[7]. Understanding THz Δn lends insight into the materials and provides information for applications in THz devices and systems.

THz, as contactless and nonionizing, is emerging as an attractive probe into structure in electrically insulating materials, compared with other approaches [12]-[15]. Because THz waves penetrate such materials, THz can provide internal structure. Birefringence is probed by various optical methods [16]-[19]. However, due to the opacity at visible and near-IR wavelengths, THz approaches are attractive to provide insight into underlying anisotropy [20].

In this letter, we obtain the polarization-dependent refractive index n from 100 GHz to 2.5 THz in NP Al_2O_3 films using THz methods. Due to its trigonal structure, NP Al_2O_3 shows uniaxial THz birefringence, which is comparable with earlier values from Fourier-transform spectroscopy.

Eight NP Al_2O_3 films on Al were studied (Table 1). A two-step (2S) anodization (AN) forms a uniform film giving a relatively homogeneous self-organized NP lattice compared with single-step AN [21] (Fig. 1). Before AN, the substrates are electrochemically polished in a mixed solution of perchloric acid and ethanol (1:5 in vol.) at 20 V for 60 s. After polishing, a mirror-like Al surface with striations is visible to the eye. NP Al_2O_3 films are formed by a 2S AN. The first AN is done for template formation at 3 ^{o}C and 40 V bias. In the first AN, 0.3 M $H_2C_2O_4$ is used as an electrolyte. Next the sample is etched in a mixture of 0.2 M Cr_2O_3 and 0.4 M orthophosphoric acid electrolyte at 65 ^{o}C for 4 hrs to remove the oxide layer formed during the first AN, leaving behind a regular pattern of etching pits acting as a template for subsequent NP formation for the second AN [22]. The second AN is done with the same apparatus and conditions as the first. The NP Al_2O_3 film thickness is controlled by adjusting AN time, and the regularity of long pore channels are not affected [23]. The pore arrangement, such as diameter and interpore distance, and structural features of the NP Al_2O_3 film formed after AN were characterized using FE-SEM images, in Fig. 2. Pore diameter is defined as that of the circular holes formed on the Al_2O_3 film, and inter-pore distance is that between one edge of the pore to the other edge of a neighboring pore.

Table 1. Summary of the eight samples. Sample 8 is a bare Al substrate subjected to electrochemical polishing only.

Sample	Anodization	Duration of 2nd Anodization (hr)	Film Thickness by FE-SEM $d_{Al_2O_3}$ (μm)
1	1	/	80
2	1+2	30	90
3	1+2	6.5	20
4	1+2	8	30
5	1+2	16	50
6	1+2	20	60
7	1+2	4	12
8	N/A	N/A	N/A

A hexagonal lattice of NPs with interpore distance 105 ± 5 nm and pore diameter 33 ± 3 nm is characterized by FE-SEM for samples after the second AN. Because of the delicacy of the film structure, a noncontact approach, as is the case of THz imaging, is required for its investigation.

Reflective THz experiments are carried out with a TeraView TPS Spectra 3000 as described in in Ref. [24].

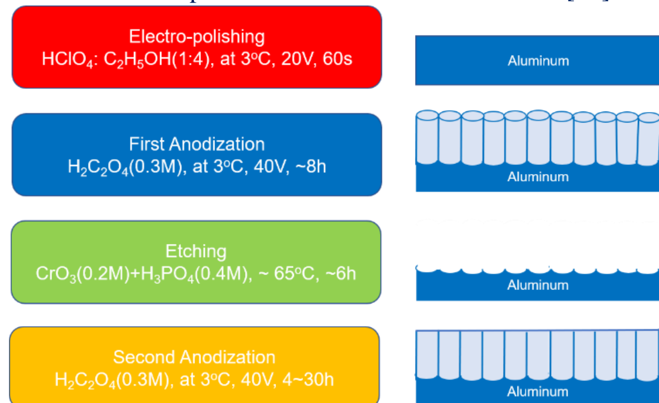

Fig. 1. 2S AN. Left column shows process flow; right column schematic of the cross section through the surface including the NP Al_2O_3 film.

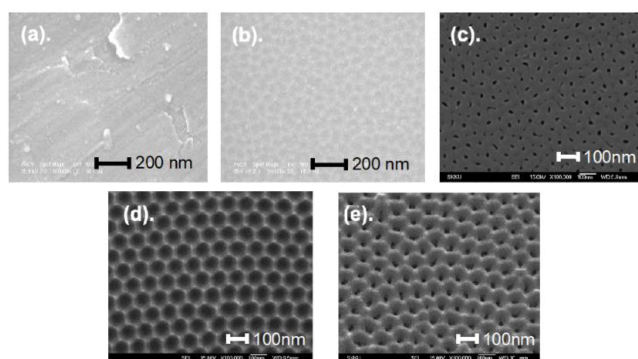

Fig. 2 Top view FE-SEM images of sample: (a) raw Al foil, (b) after electro-polishing, (c) after first AN, (d) after etching, and (e) after second AN.

The roughly single-cycle reference pulse produced by the apparatus is characterized by measuring its temporal profile after reflecting it off a piece of polished steel or Al. We then proceed with the THz reflection measurement of the sample. In reflection, we obtain two temporally overlapped echoes, one from the air/NP Al_2O_3 and one from the NP Al_2O_3/Al interface. The time delay between the two and the film thickness from destructive measurements on a single sample enables us to extract the approximate film refractive index—without reference to polarization. From the refractive index, we can then obtain the extracted film thicknesses for the other samples. We next carry out polarization-resolved THz reflectivity experiments to accurately obtain the polarization-dependent refractive index and Δn.

Optical microscopy at 50x of all films was carried out (not shown) to understand the macro/mesoscopic nature of the surface after NP Al_2O_3 film growth. All samples evidenced surface striations aligned at ~73° with respect to the horizontal edges of the rectangular samples and are rolling marks; Al substrates are polycrystalline as evidenced by x-ray diffraction (XRD). Striation direction may be connected to Δn observed below. Crystal structure was examined by x-ray diffraction (HR-XRD) (Panalytical X'pert Pro MRD with Cu Kα radiation in triple-axis mode); diffractograms of bare Al (sample 8), single- (sample 1), and 2S AN (sample 2) Al_2O_3 films are shown in Fig. 3. In all cases peaks appear at 2θ=44.5° and 78° associated with the cubic Al substrate. After the first and second AN, peaks occur at 2θ = 38.5° indicating tetragonal Al_2O_3 [25]. The conducting Al substrates result in strong THz reflection [26]. This is also confirmed by the negligible polarization dependence of the reflections from sample 8. Figure 4 shows the polarization dependence of the reflected signals from 80° to 90° for sample 1, which was subjected only to the first AN. It is apparent that the first echo reflected from top air/NP Al_2O_3/Al interface is broad and weak and is not readily distinguished from background noise. Cross-sectional FE-SEM of sample 1 (Fig. 5) shows a nonuniform 20-μm thick NP Al_2O_3 top layer adjacent to air above a uniform 60-μm NP Al_2O_3 layer between the nonuniform NP Al_2O_3 top layer and the Al substrate. The top layer may result from heat generated on the surface of the electrolyte due to the high AN voltage [27]. Due to the fact that the air/NP Al_2O_3 interface is far from smooth within the transverse focus (~300 m) and due to scattering at and within the 20-µm nonuniform Al_2O_3 top layer itself, a small first echo appears ahead of the strong echo reflected from the highly reflective NP Al_2O_3/Al interface.

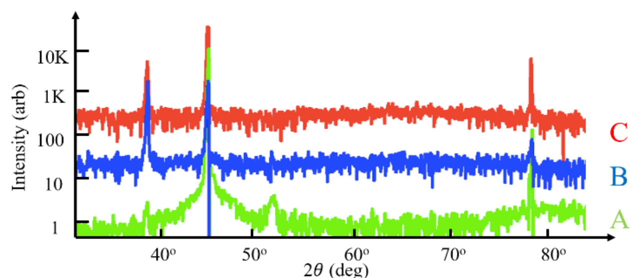

Fig. 3. X-ray diffractograms of (A) Al, (B) first AN Al_2O_3, and (C) 2S AN Al_2O_3 films.

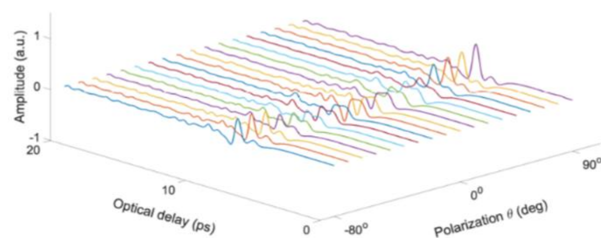

Fig. 4 Reflected THz signal for various polarization angles for sample 1.

The second AN results in a far more regular NP-lattice

seeded by the first as shown in cross-section and top-view FE-SEM in Figs. 2 and 5. For samples 2-7 produced by 2S AN, while the lattice constant is too small to resolve in THz images, THz polarization anisotropy is also expected. Figure 6 shows the reflected THz signals with various polarizations for sample 2, the results for which are representative of all samples produced by the 2S AN. Due to the relative smoothness of the top air/NP Al_2O_3 interface (height variation 45 nm from FE-SEM), scattering from this interface is negligible. Two positive echoes, the first corresponding to the THz signal reflected from the top air/NP Al_2O_3 interface and the second from the NP Al_2O_3/Al interface are seen clearly.

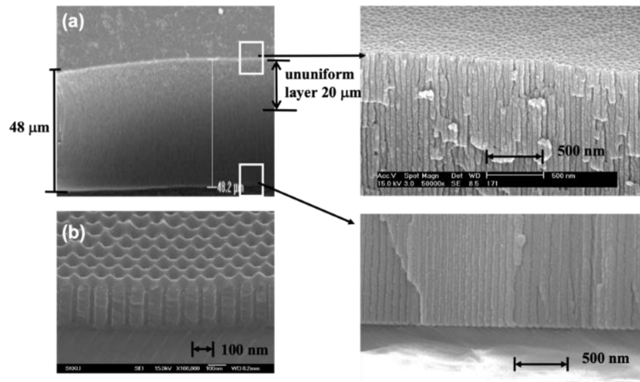

Fig. 5 Cross-sectional FE-SEM image after the (a) first (sample 8) and (b) 2S AN. In (a) we see a relatively irregular lattice and a rough air/NP Al_2O_3 interface; (b) shows much greater regularity.

The time delay ΔT between the echoes depends on the thickness $d_{Al_2O_3}$ and refractive index n of the NP Al_2O_3 film via $n = c\Delta t/(2d_{Al_2O_3})$; c is the *in-vacuo* speed of light.

We treat the NP Al_2O_3 film as an effective medium since the NPs are far smaller than the wavelength (~100 µm) in the usable THz bandwidth and neglect dispersion. Also, in order to assess n, we must begin with a sample of known thickness d_{layer}. The polarization-dependent refractive indices are shown in Fig. 7 along with a fit to $A\ \sin(2\theta + \varphi_1)+B\ \sin(6\theta + \varphi_2)+C$. The first term describes Δn, while the second term reflects any effect of the hexagonal lattice. We find A = 1.36 and B = -0.335 and conclude B is not significant; the polarization anisotropy does not appear to track the NP lattice. We find φ_1 = 80° for which the polarization is aligned parallel to the roll marks, and the ordinary refractive index is $n_o = 3.5$; the extraordinary refractive index is $n_e = 3.2$. Similar results are obtained for samples 3-7 also processed with 2S AN. It is not clear if this similarity in directions is fortuitous or if the roll marks influence the optical properties of the NP Al_2O_3 films. In principle, based on Eq. (1), n_o and n_e are obtained once the orientation of the respective axes align parallel to the incident THz polarization. Birefringence for the NP Al_2O_3 film can also be calculated based on the orientation of the optical axis, which is Δn = -0.3, close to the value reported for Al_2O_3 reported elsewhere [28][30]. (Although Δn was not studied In Ref. [30][30], refractive indices of Al_2O_3 in the THz range slightly larger than 3 were reported).

The NP structure means that the films are a mixture of air and Al_2O_3. In Ref. [31], n of NP Al_2O_3 films was characterized in the visible and NIR regions of the spectrum. The films have air volume fill factors f from 4 to 22 %. The measured values of n were significantly less than for bulk and this was accounted for using Maxwell-Garnett (MG) theory. For us f = 9 %. While the NPs and the NP lattice constants themselves are small on the THz wavelength scale, we do not expect appreciable photonic-crystal effects, suggesting that, neglecting Δn, the refractive indices should be well predicted by MG theory. Neglecting Δn, for propagation along the axis of the air-filled holes (specular direction), the effective refractive indices of NP Al_2O_3 are $n_i = n_{i,\text{Al2O3}}[(1+\Gamma_i)/(1-\Gamma_i)]^{1/2}$, where $\Gamma_i = f(1 - n_{i,\text{Al2O3}}^2)/(1+n_{i,\text{Al2O3}}^2)$ [31], where $i = \parallel, \perp$, and $n_{i,\text{Al2O3}}$ is the refractive index of bulk Al_2O_3. Putting $n_{\parallel,\text{Al2O3}}$ = 3.39 and $n_{\perp,\text{Al2O3}}$ = 3.07 [28], we find $n_\parallel$ = 3.14 and $n_\perp$ = 2.85. Note, however, Δn = 0.29, which is close both to the value for bulk Al_2O_3 and to the value we measure.

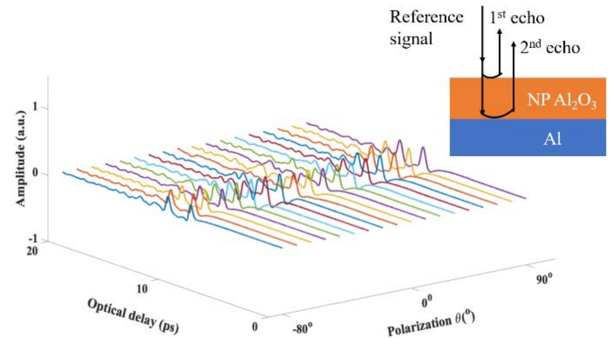

Fig. 6. Reflected THz signal for various polarization angles for sample 2. Inset shows the origin of the two echoes in the reflected THz signal: one from the air/NP Al_2O_3 interface and the second from the NP Al_2O_3/Al interface.

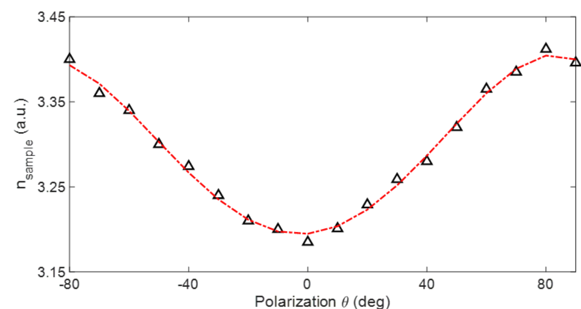

Fig. 7. Calculated refractive index of the NP Al_2O_3 film as a function of polarization for sample 2.

Next, film thickness of samples 2-7 is measured by reflective pulsed THz tomography. As mentioned above, the echoes arising from the air/Al_2O_3 and Al_2O_3/Al interfaces strongly overlap in time and cannot be visually distinguished.

Deconvolution is essential to extract the time delay between the two echoes as well as to identify meaningful features in a background of noise. We use sparse deconvolution (SD), as described in Ref. [32]. The idea behind SD is that for a stratified medium the impule response function $h(t)$ is a sequence of peaks with zero in between; $h(t)$ gives the reflected signal expected with very short incident pulses; Δt, the time between successive peaks in $h(t)$, and n give $d_{Al_2O_3}$ as discussed above. The sparsity assumption is thus additional information we have about the samples that supplements the measured reflected signal and enables us to extract the time delay even if the corresponding optical thickness of the film is close to or somewhat below the axial resolution limit.

The reflected signal $r(t)$ from samples 2-7 with NP Al_2O_3 layers of various $d_{Al_2O_3}$ and the corresponding $h(t)$ reconstructed by SD are shown in Fig. 11. Two positive peaks are observed, the first corresponding to the position of air/NP Al_2O_3 interface and the second to the NP Al_2O_3/Al interface. The amplitude of the second peak is larger due to the strong reflection from the dielectric/metal interface. The optical delay between the two peaks can be used to estimate $d_{Al_2O_3}$. Even for sample 7, with $d_{Al_2O_3}$=12 μm, a weak peak [arrow in Fig. 11(f)] can be seen that overlaps with the strong peak due to the NP Al_2O_3/Al interface. As for sample 1, due to scattering and possibly dispersion occurring in the 20 µm top nonuniform Al_2O_3 layer, the signal reflected from NP Al_2O_3/Al interface is weak and broad, thereby degrading the performance of SD.

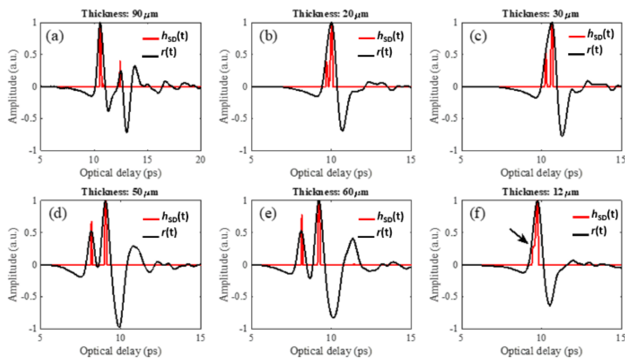

Fig. 8. $h_{SD}(t)$ reconstructed by SD (red) and the reflected THz signal $r(t)$ (black) for samples 2-7. The arrow in (f) indicates the position of the feature in h(t) reconstructed from SD associated with the air/NP Al_2O_3 interface.

Table 2. Thicknesses of NP Al_2O_3 films (samples 2-7). First column is nominal thickness of NP Al_2O_3 from cross-sectional FE-SEM. Second and third columns (sampled at 20 random pixels) are obtained from relevant peaks in $h_{SD}(t)$. The low standard deviations confirm high film uniformity as well as robustness of THz-based estimates.

Sample	Nominal Film Thickness $d_{Al_2O_3}$ (μm)	Mean $d_{Al_2O_3}$ Measured by THz Tomography (μm)	Standard Deviation of $d_{Al_2O_3}$ by THz Tomography (μm)
2	90	87	2.4
3	20	19.3	1.3
4	30	27.9	1.9
5	50	50.6	2.6
6	60	61.4	2.4
7	12	13.3	0.7

Lastly, the uniformity of the NP Al_2O_3 film thickness is also investigated among samples 2-7 through selecting 20 pixels randomly from the entire NP Al_2O_3 region, and the minimum distance between two selected pixels is 0.5 mm. Table 2 shows $d_{Al_2O_3}$ in samples 2-7. We see that the mean thickness agrees well with the value measured by destructive cross-sectional measurements. Low standard deviation indicates high uniformity of the NP Al_2O_3 films as well as the robustness of SD and the stability of the THz measurement.

THz Δn of NP Al_2O_3 films on Al foil is measured. The ordinary and extraordinary refractive indices of the NP Al_2O_3 films are $n_o = 3.5, n_e = 3.2$, leading to a Δn = -0.3, in good agreement with the literature. We then measured the NP Al_2O_3 film thicknesses nondestructively using a super-resolution reconstruction based on SD, and find values in good agreement with those obtained from optical microscopy.

Funding

We gratefully acknowledge the support of ArcelorMittal, Conseil Régional Grand Est, and CPER SusChemProc.

Disclosures

The authors declare no conflicts of interest.

References and links

1. V. N. Bogomolov, S. V. Gaponenko, I. N. Germanenko, A. M. Kapitonov, E. P. Petrov, N.V. Gaponenko, A.V. Prokofiev, A.N. Ponyavina, N.I. Silvanovich, and S.M. Samoilovich, Phys. Rev. E **55**, 7619 (1997).
2. I. Nikolaev, P. Lodahl, and W. L. Vos, Phys. Rev. A **71**, 1 (2005).
3. S. Ono, and N. Masuko, Surf. Coat. Tech. **169-170**, 139 (2003).
4. W. Lee, R. Ji, U. Gosele, and K. Nielsch, Nat. Mater. **5**, 741 (2006).
5. M. Shaban, H. Hamdy, F. Shahin, J. Park, and S.W. Ryu, J. Nanosci. Nanotechnol. **10**, 3380 (2010).
6. B. Scherger, M. Scheller, N. Vieweg, S.T. Cundiff, and M. Koch, Opt. Express **19**, 24884 (2010).
7. M.E. Reid, and R. Fedosejevs, Appl. Opt. **45**, 2766 (2006).
8. T.M. Todoruk, I.D. Hartley, and M.E. Reid, IEEE. Trans. Terahertz Sci. Technol. **2**, 123 (2011).
9. A.A. Lutich, M.B.Danailov, S. Volchek, V.A. Yakovtseva, V.A. Sokol, and S.V. Gaponenko, Appl. Phys. B **84**, 327 (2006).
10. D. Grischkowsky, S. Keiding, M. van Exeter, and C. Fattinger, J. Opt. Soc. Am. B. **7**, 2006 (1990).
11. Y. Kim, J. Ahn, B. G. Kim, and D. S. Yee, Jpn. J. Appl. Phys. Lett. **50**, 030203 (2011).
12. C.D. Stoik, M.J. Bohn, and J.L. Blackshire, Opt. Express **16**, 17039 (2008).
13. K. Inaba, The Rigaku Journal **24**, 10 (2008).
14. M. Wormington, C. Panaccione, K.M. Matney, and D.K. Bowen, Phil. Trans. R. Soc. Lond. A **357**, 2827 (1999).
15. A. Gallego, J.F. Gil, E. Castro, and R. Piotrkowski, Surf. Coat. Technol. **201**, 4743 (2007).
16. K. Ramesh, *Digital Photoelasticity* (Springer, Berlin, 2000).
17. H. Fujiwara, *Spectroscopic ellipsometry: Principle and applications* (John, Wiley & Sons, 2007).
18. D. Stifter, Appl. Phys. B **88**, 337 (2007).
19. J.J. Senkevich, S.B. Desu, and V. Simkovic, Polym. J. **41**, 2379 (2000).
20. L.L. Zhang, H. Zhong, C. Deng, C. Zhang, and Y.J. Zhao, Appl. Phys. Lett. **94(21)**, 211106 (2009).

21. A.P. Li, F. Muller, A. Birner, K. Nielsch, and U. Gosele, J. Appl. Phys. **84**, 6023-6026 (1998).
22. G.D. Sulka and W.J. Stepniowski, Electrochimica Acta.**54**, 3683 (2009).
23. F. Li, L. Zhang and R.M. Metzger, Chem. Mater. **10**, 2470 (1998).
24. J. Dong, A. Locquet, and D.S. Citrin, J. Infrared Millim. Terahertz Waves **37**, 289 (2016).
25. M.S. Ilando, A. Mutalikdesai, and S.K. Ramasesha, J. Chem. Sci. **128**, 153 (2016).
26. N. Lamaan, and D. Grischkowsky, Appl. Phys. Lett. **93**(5), 051105 (2008).
27. H. Masuda, and K. Fukuda, Sci. **268**, 1466 (1995).
28. E. D. Palik, *Handbook of Optical Constants of Solids I*, p. 700, (1985).
29. Y. Kim, M. Yi, B G. Kim, and J. Ahn, Appl. Opt. **50**, 2906 (2011).
30. K.Z. Rajab, M. Naftaly, E.H. Linfield, J.C. Nino, D. Arenas, D. Tanner, R. Mittra, and M. Lanagan, J. Micro. and Elect. Pack. 5, 101 (2008).
31. A. Hierro-Rodriguez, P. Rocha-Rodrigues, F. Valdés-Bango, J.M. Alameda, P.A.S Jorge, J.L. Santos, J.P. Araujo, J.M. Teixeira, and A Guerreiro, J. Phys. D: Appl. Phys. **48**, 455105 (2015).
32. J. Dong, X. Wu, A. Locquet, and D. S. Citrin, IEEE Trans. Terahertz Sci. Technol. **7**, 260 (2017).

References and links

[1] V. N. Bogomolov, S. V. Gaponenko, I. N. Germanenko, A. M. Kapitonov, E. P. Petrov, N.V. Gaponenko, A.V. Prokofiev, A.N. Ponyavina, N.I. Silvanovich, and S.M. Samoilovich, "Photonic band gap phenomenon and optical properties of artificial opals," Phys. Rev. E **55**(6), 7619-7625 (1997).

[2] I. Nikolaev, P. Lodahl, and W. L. Vos, "Quantitative analysis of directional spontaneous emission spectra from light sources in photonic crystals," Phys. Rev. A **71**(10), 1-10 (2005).

[3] S. Ono, and N. Masuko, "Evaluation of pore diameter of anodic porous films formed on aluminum," Surf. Coat. Tech. **169-170**, 139-142 (2003).

[4] W. Lee, R. Ji, U. Gosele, and K. Nielsch, "Porous fabrication of long range ordered porous alumina membranes by hard anodization," Nat. Mater. **5**, 741-747 (2006).

[5] M. Shaban, H. Hamdy, F. Shahin, J. Park, and S.W. Ryu, "Uniform and reproducible barrier layer removal of porous anodic alumina membrane," J. Nanosci. Nanotechnol. **10**(5), 3380-3384, (2010).

[6] B. Scherger, M. Scheller, N. Vieweg, S.T. Cundiff, and M. Koch, "Paper terahertz wave plates," Opt. Express **19**(25), 24884-24889 (2010).

[7] M.E. Reid, and R**.** Fedosejevs, "Terahertz birefringence and attenuation properties of wood and paper," Appl. Opt. **45**(12), 2766-2772 (2006).

[8] T.M. Todoruk, I.D. Hartley, and M.E. Reid, "Origin of birefringence in wood at terahertz frequency," IEEE. Trans. Terahertz Sci. Technol. **2**(1), 123-130 (2011).

[9] A.A. Lutich, M.B.Danailov, S. Volchek, V.A. Yakovtseva, V.A. Sokol, and S.V. Gaponenko, "Birefringence of nanoporous alumina: dependence on structure parameters," Appl. Phys. B **84**(1-2), 327-331 (2006).

[10] D. Grischkowsky, S. Keiding, M. van Exeter, and C. Fattinger, "Far-infrared time-domain spectroscopy with terahertz beams of dielectrics and semiconductors," J. Opt. Soc. Am. B **7**(10), 2006-2015 (1990).

[11] Y. Kim, J. Ahn, B. G. Kim, and D. S. Yee, "Terahertz birefringence in Zinc Oxide," Jpn. J. Appl. Phys. Lett. **50**(3R), 030203 (2011).

[12] C.D. Stoik, M.J. Bohn, and J.L. Blackshire, "Nondestructive evaluation of aircraft composites using transmissive terahertz time domain spectroscopy," Opt. Express **16**(21), 17039-17051 (2008).

[13] K. Inaba, "X-ray thin film measurement techniques," The Rigaku Journal **24**(1), 10-15 (2008).

[14] M. Wormington, C. Panaccione, K.M. Matney, and D.K. Bowen, "Characterization of structures from X-ray scattering data using genetic algorithms," Phil. Trans. R. Soc. Lond. A **357**(1761), 2827-2848 (1999).

[15] A. Gallego, J.F. Gil, E. Castro, and R. Piotrkowski, "Identification of coating damage processes in corroded galvanized steel by acoustic emission wavelet analysis," Surf. Coat. Technol. **201**(8), 4743-4756 (2007).

[16] K. Ramesh, *Digital Photoelasticity* (Springer, Berlin, Heidelberg, 2000).

[17] H. Fujiwara, *Spectroscopic ellipsometry: Principle and applications* (John Wiley & Sons, 2007).

[18] D. Stifter, "Beyond biomedicine: a review of alternative applications and developments for optical coherence tomography," Appl. Phys. B **88**(3), 337-357 (2007).

[19] J.J. Senkevich, S.B. Desu, and V. Simkovic, "Temperature studies of optical birefringence and X-ray diffraction with poly(p-xylylene), poly(chloro-p-xylylene) and poly (tetrafluoro-p-xylylene) CVD thin films," Polym. J. **41**(7), 2379-2390 (2000).

[20] L.L. Zhang, H. Zhong, C. Deng, C. Zhang, and Y.J. Zhao, "Polarization sensitive terahertz time-domain spectroscopy for birefringence materials," Appl. Phys. Lett. **94(21)**, 211106 (2009).

[21] A.P. Li, F. Muller, A. Birner, K. Nielsch, and U. Gosele, "Hexagonal pores arrays with a 50-420 nm interpore distance formed by self-organization in anodic alumina," J. Appl. Phys. **84**(11), 6023-6026 (1998).

[22] G.D. Sulka and W.J. Stepniowski, "Structural features of self-organized nanopore arrays formed by anodization of aluminum in oxalic acid at relatively high temperatures," Electrochimica Acta **54**(14), 3683-3691 (2009).

[23] F. Li, L. Zhang and R.M. Metzger, "On the growth of highly ordered pores in anodized aluminum oxide," Chem. Mater. **10**(9), 2470-2480 (1998).

[24] J. Dong, A. Locquet, and D.S. Citrin, "Enhanced terahertz imaging of small forced delamination in woven glass fibre-reinforced composites with wavelet de-noising," J. Infrared Millim. Terahertz Waves **37**(3), 289-301 (2016).

[25] M.S. Ilando, A. Mutalikdesai, and S.K. Ramasesha, "Anodization of aluminum using a fast two-step process," J. Chem. Sci. **128**(1), 153-158 (2016).

[26] N. Lamaan, and D. Grischkowsky, "Terahertz conductivity of thin metal films," Appl. Phys. Lett. **93**(5), 051105 (2008).

[27] H. Masuda, and K. Fukuda, "Ordered metal nanohole arrays made by a two-step replication of honeycomb structures of anodic alumina," Sci. **268**(5216), 1466-1468 (1995).

[28] E. D. Palik, *Handbook of Optical Constants of Solids I*, p. 700, (1985).

[29] Y. Kim, M. Yi, B G. Kim, and J. Ahn, "Investigation of THz birefringence measurement and calculation in Al_2O_3 and $LiNbO_3$," Appl. Opt. **50**(18), 2906-2910, (2011).

[30] K.Z. Rajab, M. Naftaly, E.H. Linfield, J.C. Nino, D. Arenas, D. Tanner, R. Mittra, and M. Lanagan, "Broadband Dielectric Characterization of Aluminum Oxide (Al2O3)," J. Micro. and Elect. Pack. 5, 101–106 (2008).

[31] A. Hierro-Rodriguez, P. Rocha-Rodrigues, F. Valdés-Bango, J.M. Alameda, P.A.S Jorge, J.L. Santos, J.P. Araujo, J.M. Teixeira, and A Guerreiro, "On the anodic aluminium oxide refractive index of nanoporous templates," J. Phys. D: Appl. Phys. **48**, 455105-455110 (2015).

[32] J. Dong, X. Wu, A. Locquet, and D. S. Citrin, "Terahertz superresolution stratigraphic characterization of multilayered structures using sparse deconvolution," IEEE Trans. Terahertz Sci. Technol. **7**(3), 260-267 (2017).